

Influence of stacking fault energy on nanostructure formation under high pressure torsion

Y.H. Zhao^a, X.Z. Liao^a, Y.T. Zhu^{a,*}, Z. Horita^b, T.G. Langdon^c

^a Materials Science and Technology Division, Los Alamos National Laboratory, MS G755, Los Alamos, NM 87545, USA

^b Department of Materials Science & Engineering, Faculty of Engineering, Kyushu University, Fukuoka 812-8581, Japan

^c Departments of Aerospace & Mechanical Engineering and Materials Science, University of Southern California, Los Angeles, CA 90089-1453, USA

Received in revised form 30 June 2005

Abstract

Copper, bronze (Cu–10 wt.% Zn) and brass (Cu–30 wt.% Zn) were deformed by high pressure torsion (HPT) under a pressure of 6 GPa for five rotations. The stacking fault energies (SFEs) of copper, bronze and brass are 78, 35 and 14 mJ/m², respectively, and their average grain sizes after the HPT processing were about 84, 54 and 17 nm, respectively. Deformation twins were found in all samples and their densities increased with decreasing SFE. This work demonstrates that under the same conditions of HPT a low SFE promotes the formation of nanostructures and deformation twins.

© 2005 Elsevier B.V. All rights reserved.

Keywords: Stacking fault energy; Copper and copper alloys; High pressure torsion; Microstructure; Deformation twins

1. Introduction

Severe plastic deformation (SPD) is one of the most promising approaches to synthesize fully dense, contamination-free nanostructured (NS) materials. In this approach, conventional coarse-grained (CG) materials are deformed plastically to a very large strain to produce substantial grain refinement and, under some conditions, grain sizes within the nanometer range. Techniques of SPD processing include mechanical milling (MM) [1], equal-channel angular pressing (ECAP) [2–4], high pressure torsion (HPT) [3,5,6], accumulative roll-bonding (ARB) [7], repetitive corrugation and straightening (RCS) [8,9] and their combinations [10–13]. Among all of these techniques, the results to date suggest that only HPT is capable of producing bulk NS materials with grain sizes below 100 nm [14–17].

In the SPD approach, it is commonly found that the mean crystallite size (or subgrain size, dislocation cell size) of the deformed materials decreases with imposed strain and reaches a minimum steady-state value (d_{\min}). Experimental observations, primarily from MM processing, show that d_{\min} scales inversely

with the melting point of the metal and decreases at lower processing temperatures [1]. Recently, Mohamed [18] developed a dislocation model that relates d_{\min} during MM processing with several material parameters including the stacking fault energy (SFE), hardness, self-diffusion activation energy, melting temperature and shear modulus. The model appears to agree well with experimental data reported for MM-processed materials. However, there is a potential problem with MM processing because there may be contamination from the milling media and/or the ambient atmosphere and this may significantly affect the value recorded for d_{\min} .

The objective of this work is to investigate the effect of SFE on nanostructure formation and the value of d_{\min} in HPT processing. An advantage of using HPT is that it can produce bulk NS materials with grain sizes below 100 nm but without introducing any inherent contamination. The experiments were conducted using Cu, Cu–10 wt.% Zn and Cu–30 wt.% Zn samples, which have the same fcc single phase crystal structure but different SFEs of 78 [19,20], 35 and 14 mJ/m² [19,21], respectively. The SFE of Cu was estimated using the stacking-fault tetrahedral stability method [20]. The SFEs of Cu–10 wt.% Zn and Cu–30 wt.% Zn were measured from observations of dislocation nodes with the measurement errors within 10% [21]. The overall objective of this study was to compare the experimental results with the model of Mohamed [18].

* Corresponding author. Tel.: +1 505 667 4029; fax: +1 505 667 2264.
E-mail address: yzhu@lanl.gov (Y.T. Zhu).

2. Experimental procedures

2.1. Sample preparation

The materials were obtained in the form of rods having diameters of 10 mm for copper (99.9%) and brass (Cu–30 wt.% Zn) and in the form of plates with a thickness of 6 mm for bronze (Cu–10 wt.% Zn). They were sliced to disks having thicknesses of 0.8 mm and diameters of 10 mm. These disks were subjected to HPT at room temperature for five rotations at a speed of 1 rotation/min under an imposed pressure of 6 GPa. The processing was performed using the facility described elsewhere [22] where the sample is placed between a stationary upper and a rotational lower Bridgman anvil.

2.2. Transmission electron microscopy

Conventional transmission electron microscopy (TEM) and high-resolution TEM were performed on a Phillips CM30 microscope operating at 300 kV and a JEOL 3000F microscope operating at 300 kV. TEM specimens were cut at a distance of 4 mm from the disk center and therefore near the outer edge of each disk. At this distance from the center, the shear strain imparted by HPT is about 160 and the equivalent strain is about 90. It should be noted that, in practice, the imposed strain is probably lower than these values because of potential slipping between the sample disks and the anvil. The specimens were thinned to about 10 μm by mechanically grinding both sides of the disks using diamond-lapping films (in the order of 30, 6, 1 and 0.1 μm). Further thinning to a thickness of electron transparency was carried out using a Gatan Dual Ion Milling System with an Ar⁺ accelerating voltage of 4 kV and liquid nitrogen for cooling the specimen. It should be noted that the current conventional TEM and high-resolution TEM measured the microstructural information on the sample disk plane (from the top view of the HPT disks).

2.3. X-ray diffraction

Quantitative X-ray diffraction (XRD) measurements of the HPT-processed disks were performed on a Scintag X-ray diffractometer equipped with a Cu target operating at 1.8 kW and a graphite curved single-crystal $\langle 0002 \rangle$ monochromator in order to select the Cu K α radiation at the goniometer receiving slit section. The divergence and anti-scattering slits were chosen to be 0.5° and 0.5°, respectively, and the receiving slit had a width of 0.3 mm. θ – 2θ scans were performed to record the XRD patterns at room temperature. Pure Al powder (99.999%) was annealed at 200 °C in Ar and used as an XRD peak-broadening reference for the average grain size and microstrain calculations. The peak parameters (peak intensity, peak-maximum position, full width at half maximum and integral breadth) were determined by fitting a Pearson VII function to the measured peaks. Unlike conventional TEM and high-resolution TEM, the XRD results were averaged from the whole disk sample and represent the microstructural information along the cross-sectional direction of the HPT-processed disks.

Table 1

A list of the XRD-measured average grain sizes (d_{XRD}), grain sizes (d_{111} and d_{200}) along $\langle 111 \rangle$ and $\langle 200 \rangle$ directions, the average grain size from TEM measurements (d_{TEM}), lattice parameters (a), SFEs (γ) [19–21], absolute values of Burgers vectors (b) and shear modulus (G) [26] of HPT-processed Cu, Cu–10 wt.% Zn and Cu–30 wt.% Zn alloys

Samples	Copper (99.9% Cu)	Bronze (Cu–10 wt.% Zn)	Brass (Cu–30 wt.% Zn)
d (nm)			
d_{111}	62	44	15
d_{200}	106	64	19
d_{XRD}	84	54	17
d_{TEM}	75	50	10
a (Å)	3.619	3.641	3.691
γ (mJ/m ²)	78	35	14
b (nm)	0.2559	0.2575	0.2610
G (MPa)	48.3	46.5	40.1

The errors of the XRD-measured grain sizes are about 15 nm for Cu and Cu–10 wt.% Zn, and about 5 nm for Cu–30 wt.% Zn. The errors of TEM-measured grain sizes are about 20 nm for Cu and Cu–10 wt.% Zn, and about 3 nm for Cu–30 wt.% Zn. The errors of the XRD-measured lattice parameters are about 0.005 Å.

3. Experimental results

The grain sizes of the HPT-processed samples were measured from the XRD peak broadening [23]. Because of the existence of a $\{111\}$ texture, it is possible only to calculate the grain sizes (d_{111} and d_{200}) using the pairs of (111) – (222) and (200) – (400) reflections, as listed in Table 1 and shown in Fig. 1. The mean grain sizes, d_{XRD} , were averaged from d_{111} and d_{200} . As demonstrated in Table 1, a decrease in the SFE from 78 to 14 mJ/m² (from copper to brass) leads to a corresponding decrease in the average grain sizes measured by XRD from 84 ± 15 to 17 ± 5 nm. Moreover, it is apparent that the grain size is anisotropic. For example, d_{200} of the HPT-processed Cu

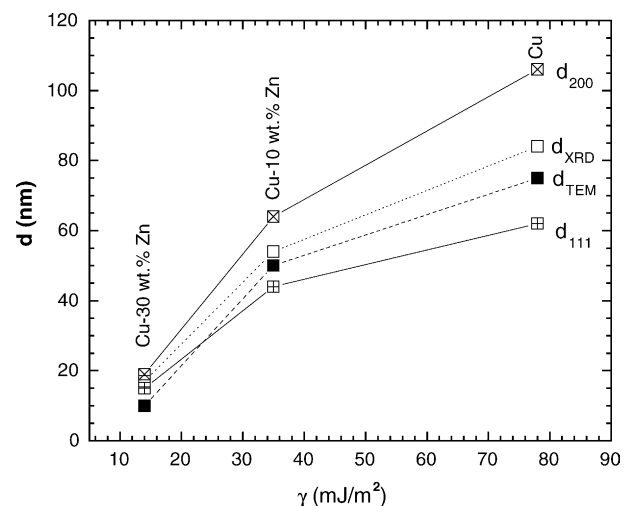


Fig. 1. XRD-measured grain sizes (d_{111} and d_{200}) along $\langle 111 \rangle$ and $\langle 200 \rangle$ directions, the mean grain size (d_{XRD}) averaged from d_{111} and d_{200} , and the TEM-measured average grain sizes for HPT-processed Cu and Cu–Zn alloys. The errors of the XRD-measured grain sizes are about 15 nm for Cu and Cu–10 wt.% Zn, and 5 nm for Cu–30 wt.% Zn. The errors of TEM-measured grain sizes are about 20 nm for Cu and Cu–10 wt.% Zn, and 3 nm for Cu–30 wt.% Zn.

(106 ± 15 nm) is much larger than d_{111} (62 ± 15 nm). Fig. 1 also shows that the difference between d_{111} and d_{200} decreases with decreasing SFE. For the HPT-processed Cu–30 wt.% Zn, the value of d_{200} (19 ± 5 nm) is very close to d_{111} (15 ± 5 nm) indicating that equiaxed grains were formed in the low SFE brass.

The average grain sizes at the edge of the HPT-processed disks were determined by TEM, d_{TEM} , using the linear intercept method and measuring about 300 grains for each sample. As shown in Fig. 1, the values of d_{TEM} follow the same trend as d_{XRD} but they are slightly smaller. Generally, the grain sizes measured by TEM are larger than those measured by XRD because the X-rays measure the size of the subgrain structures [24]. The unusual trend recorded here is because the values determined from XRD relate to the whole disk and reflect the values from a cross-sectional view, while the TEM observations were conducted only at the disk edges where the grains are finest and reflect values from the top view. The presence of non-uniform grain sizes is a consequence of the intrinsic nature of HPT processing which subjects the sample disk to a higher strain at points furthest removed from the disk center [5,6,17].

Fig. 2 shows the statistical grain size distributions of the HPT-processed Cu (Fig. 2a), Cu–10 wt.% Zn (Fig. 2b) and Cu–30 wt.% Zn (Fig. 2c). It can be seen that, with decreasing SFE, the average grain size is decreased and also the width of the grain size distribution is reduced. This means that the grain structure becomes more uniform with decreasing SFE.

Fig. 3 shows representative TEM micrographs taken from the edges of HPT-processed disks of: (a) copper, (b) bronze and (c) brass. For all three samples, it is apparent that the HPT process produced equiaxed grains with random orientations. Close inspection suggests that the isotropic grain size observed in HPT-processed Cu (Fig. 3a) is inconsistent with the X-ray results. The reason for this apparent difference is that the TEM micrograph only shows the grains in the sample disk plane and the grains are probably thinner and elongated when viewed from a sample section parallel to the disk normal [25]. It is obvious from Fig. 3 that the grain size becomes smaller from copper to bronze to brass, corresponding to the decrease in the SFE.

High-resolution TEM observations in numerous areas indicate that, as the SFE decreases from copper to bronze to brass, the deformation twin density becomes higher and the width of

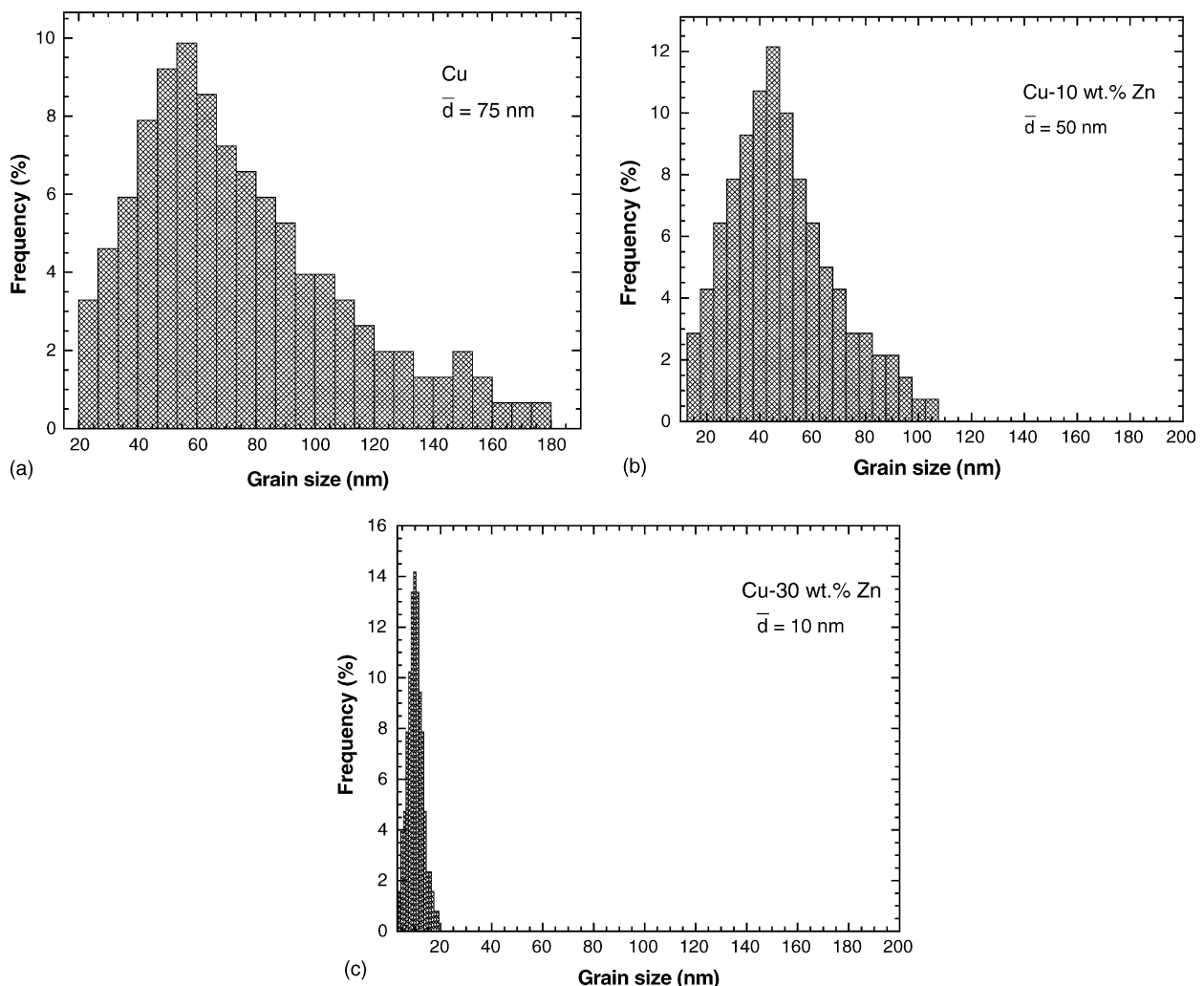


Fig. 2. Statistical distributions of grain sizes after HPT processing for: (a) copper, (b) bronze and (c) brass. The linear intercept method was used to measure the grain sizes, and about 300 grains were measured for each sample.

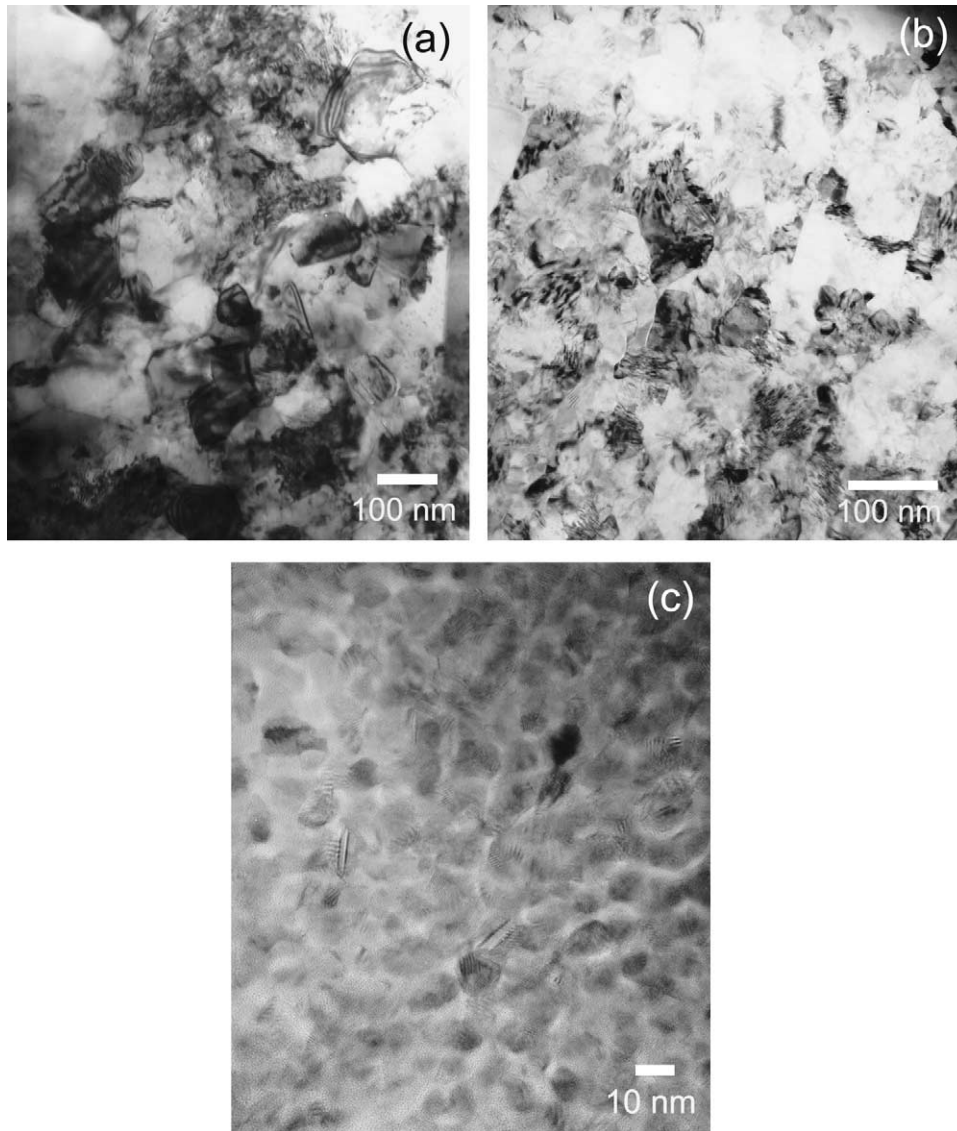


Fig. 3. Bright-field TEM micrographs at the edges of the HPT-processed disks for: (a) copper, (b) bronze and (c) brass.

deformation twins is smaller, as typically shown by Fig. 4a–c. The deformation twins in the HPT-processed Cu and bronze are mainly lamellar twins, which are emitted from the grain boundaries and terminate inside the grains (see Fig. 4b). In the HPT-processed brass, both five-fold twins and lamellar twins are observed, as represented by Fig. 4c.

4. Discussion

Extremely large strains are introduced in HPT processing and it is reasonable to anticipate that the average grain sizes measured in samples processed by HPT through five rotations correspond to the minimum grain size, d_{\min} , as defined in the model by Mohamed [18]. The experimental data in this study indicate that the SFE significantly affects the measured value of d_{\min} . The decrease in the SFE leads to a decrease in the grain sizes in the order of Cu to Cu–10 wt.% Zn to Cu–30 wt.% Zn after processing by HPT under the same experimental condition. This

trend is consistent with data observed in MM-processed metals and alloys and it is explained by the concept that d_{\min} is determined by a dynamic balance between dislocation generation and recovery [18]. Thus, a lower SFE increases the difficulty for dissociated dislocations to recombine and cross-slip, impedes the recovery process, and consequently leads to smaller values for d_{\min} . The higher twinning density with lower SFE observed in Fig. 4 is reasonable because it is well known that a lower SFE promotes deformation twinning.

It is of interest to compare the measured values of d_{\min} with the dislocation model where the relationship between d_{\min} and the SFE, γ , is given as [18]:

$$\frac{d_{\min}}{b} = A \left(\frac{\gamma}{Gb} \right)^{0.5} \quad (1)$$

where b is the absolute value of the Burgers vector, A a constant and G is the shear modulus. For a fcc structure, b is the length of unit dislocation along the $\langle 110 \rangle$ direction and equal to $\frac{\sqrt{2}}{2}a$,

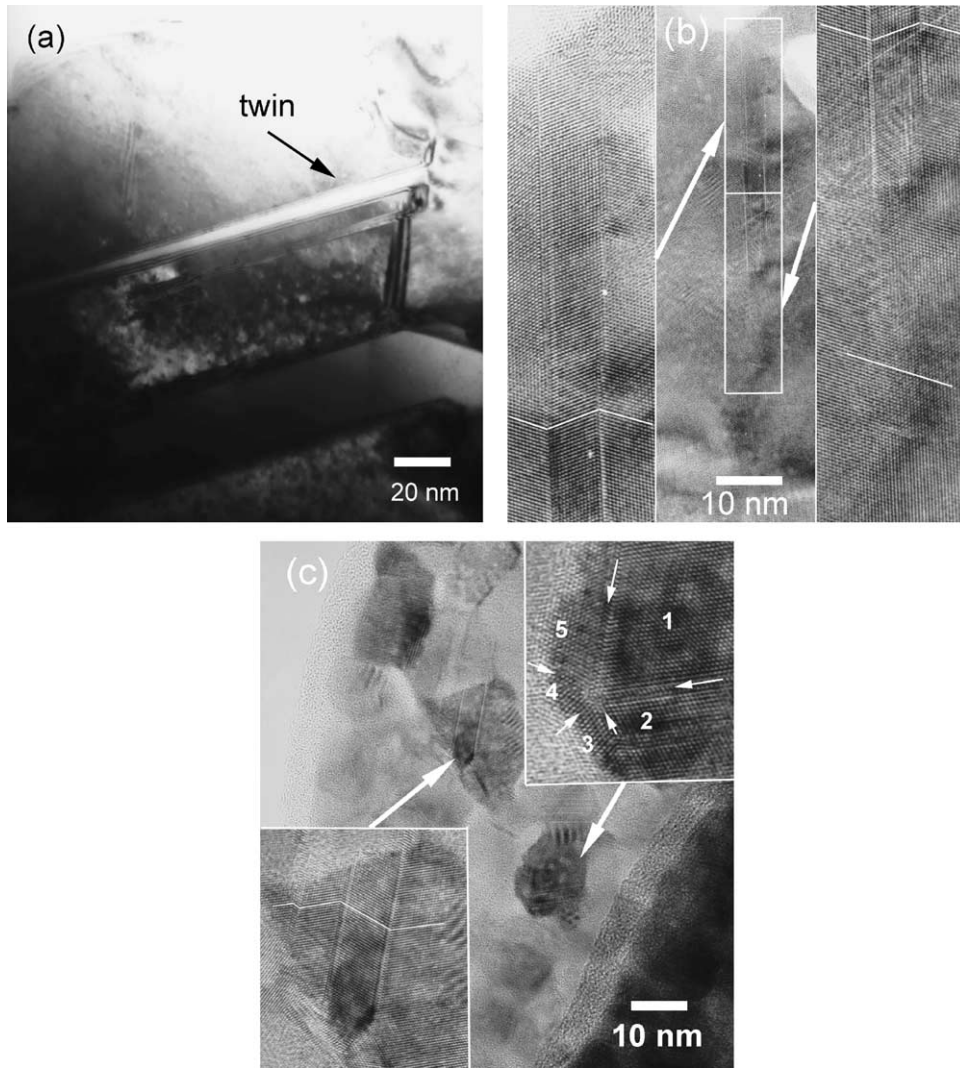


Fig. 4. Deformation twins in: (a) copper, (b) bronze and (c) brass. (b and c) High-resolution TEM images viewed from [1 1 0] direction. (b) A lamellar twin which is emitted from the grain boundary and terminate inside the grain. (c) A five-fold twin and a lamellar twin. The insets in (b and c) are the magnified images of the parts denoted by white arrows or indicated by white rectangles. The white zigzag lines in the insets in (b and c) indicate the {1 1 1} planes that form the twin relationship. The white arrows and the numbers 1–5 in the inset at the top right of (c) indicate the five-fold twin boundaries and twin domains, respectively.

where a is the lattice parameter. The values of a , b , γ [19–21] and G [26] for copper, bronze and brass are listed in Table 1.

Fig. 5 shows a plot of d_{\min}/b versus γ/Gb on a logarithmic scale using TEM and XRD data. Inspection shows that the two terms do not scale with each other in a linear way. Moreover, if it is assumed that this non-linearity is caused by a scattering in the data, it is possible to fit the data with straight lines as shown in Fig. 5 to yield slopes of 1.37 and 1.07 from the TEM and X-ray measured grain sizes, respectively. Both slopes are significantly higher than the slope of 0.5 predicted in the model as shown in Eq. (1). This disagreement is reasonable when it is noted that the model is based on the occurrence of a single deformation mechanism, whereas, as shown in Fig. 4, copper deformed primarily by lattice dislocation slip in this investigation while the Cu–30 wt.% Zn alloy deformed primarily by twinning. It is also reasonable to anticipate that, even in the same metal or alloy, the deformation mechanism may change when the grain size becomes smaller than a critical value [16,27–31].

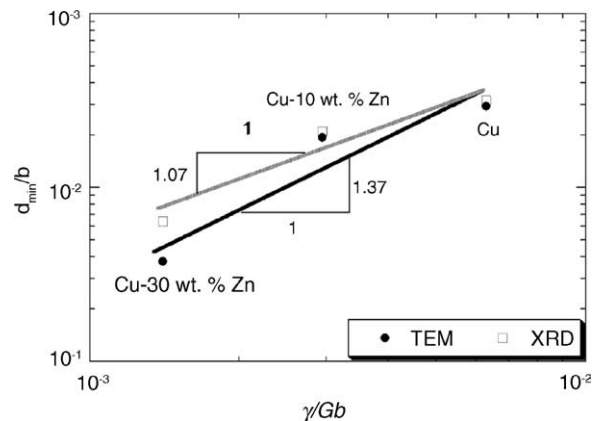


Fig. 5. Plot of d_{\min}/b vs. γ/Gb on the logarithmic scale showing that the two terms do not scale linearly and the slopes of 1.37 from the TEM results and 1.07 from the XRD values deviate significantly from the value of 0.5 predicted in Eq. (1).

5. Conclusions

Disks of Cu, Cu–10 wt.% Zn and Cu–30 wt.% Zn with different SFEs were deformed by high pressure torsion. After five rotations, their average grain sizes were found to decrease with decreasing SFE. Deformation twins were observed in all samples and the density of twins increased with decreasing SFE. The variation of the grain size with the SFE does not follow a dislocation model based on the occurrence of a single deformation mechanism. This work also demonstrates that it is feasible to adjust the SFE in order to design the structures of NS metals processed by SPD.

References

- [1] C.C. Koch, *Nanostruct. Mater.* 9 (1997) 13.
- [2] V.M. Segal, *Mater. Sci. Eng.* A197 (1995) 157.
- [3] R.Z. Valiev, R.K. Islamgaliev, I.V. Alexandrov, *Prog. Mater. Sci.* 45 (2000) 103.
- [4] M. Furukawa, Z. Horita, M. Nemoto, T.G. Langdon, *J. Mater. Sci.* 36 (2001) 2835.
- [5] H. Jiang, Y.T. Zhu, D.P. Butt, T.C. Lowe, R.Z. Valiev, *Mater. Sci. Eng.* A290 (2000) 128.
- [6] A.P. Zhilyaev, G.V. Nurislamova, B.-K. Kim, M.D. Baró, J.A. Szpunar, T.G. Langdon, *Acta Mater.* 51 (2003) 753.
- [7] Y. Saito, N. Tsuji, H. Utsunomiya, T. Sakai, R.G. Hong, *Scripta Mater.* 39 (1998) 1221.
- [8] J.Y. Huang, Y.T. Zhu, H. Jiang, T.C. Lowe, *Acta Mater.* 49 (2001) 1497.
- [9] J.Y. Huang, Y.T. Zhu, H. Jiang, T.C. Lowe, *Metall. Mater. Trans.* 32A (2001) 1559.
- [10] V.V. Stolyarov, Y.T. Zhu, T.C. Lowe, R.Z. Valiev, *Nanostruct. Mater.* 11 (1999) 947.
- [11] V.V. Stolyarov, Y.T. Zhu, T.C. Lowe, R.Z. Valiev, *Mater. Sci. Eng.* A303 (2001) 82.
- [12] V.V. Stolyarov, Y.T. Zhu, I.V. Alexandrov, T.C. Lowe, R.Z. Valiev, *Mater. Sci. Eng.* A343 (2003) 43.
- [13] A.P. Zhilyaev, B.-K. Kim, J.A. Szpunar, M.D. Baró, T.G. Langdon, *Mater. Sci. Eng.* A391 (2005) 377.
- [14] A.V. Sergueeva, C. Song, R.Z. Valiev, A.K. Mukherjee, *Mater. Sci. Eng.* A339 (2003) 159.
- [15] J.Y. Huang, Y.T. Zhu, X.Z. Liao, R.Z. Valiev, *Philos. Mag. Lett.* 84 (2004) 183.
- [16] X.Z. Liao, Y.H. Zhao, S.G. Srinivasan, Y.T. Zhu, R.Z. Valiev, D.V. Gunderov, *Appl. Phys. Lett.* 84 (2004) 592.
- [17] X.Z. Liao, Y.H. Zhao, Y.T. Zhu, R.Z. Valiev, D.V. Gunderov, *J. Appl. Phys.* 96 (2004) 636.
- [18] F.A. Mohamed, *Acta Mater.* 51 (2003) 4107.
- [19] P.C.J. Gallagher, *Met. Trans.* 1 (1970) 2429.
- [20] M.H. Loretto, L.M. Clarebrough, R.L. Segall, *Philos. Mag.* 11 (1965) 459.
- [21] A. Howie, P.R. Swann, *Philos. Mag.* 6 (1961) 1215.
- [22] G. Sakai, Z. Horita, T.G. Langdon, *Mater. Sci. Eng.* A393 (2005) 344.
- [23] Y.H. Zhao, K. Zhang, K. Lu, *Phys. Rev. B* 56 (1997) 14322; Y.H. Zhao, H.W. Sheng, K. Lu, *Acta Mater.* 49 (2001) 365; Y.H. Zhao, K. Lu, K. Zhang, *Phys. Rev. B* 66 (2002) 085404.
- [24] Y.T. Zhu, J.Y. Huang, J. Gubicza, T. Ungár, Y.M. Wang, E. Ma, R.Z. Valiev, *J. Mater. Res.* 18 (2003) 1908.
- [25] X. Huang, G. Winther, N. Hansen, T. Hebesberger, A. Vorhauer, R. Pippan, M.J. Zehetbauer, *Mater. Sci. Forum* 426–432 (2003) 2819.
- [26] E.A. Brandes, G.B. Brook, *Smithells Metals Reference Book*, seventh ed., Butterworth-Heinemann Ltd., 1992, p. 15.
- [27] M.W. Chen, E. Ma, K.J. Hemker, H.W. Sheng, Y.M. Wang, X.M. Cheng, *Science* 300 (2003) 1275.
- [28] X.Z. Liao, F. Zhou, E.J. Lavernia, S.G. Srinivasan, M.I. Baskes, D.W. He, Y.T. Zhu, *Appl. Phys. Lett.* 83 (2003) 632.
- [29] Y.T. Zhu, X.Z. Liao, S.G. Srinivasan, Y.H. Zhao, M.I. Baskes, F. Zhou, E.J. Lavernia, *Appl. Phys. Lett.* 85 (2004) 5049.
- [30] X.Z. Liao, F. Zhou, E.J. Lavernia, D.W. He, Y.T. Zhu, *Appl. Phys. Lett.* 83 (2003) 5062.
- [31] X.Z. Liao, S.G. Srinivasan, Y.H. Zhao, M.I. Baskes, Y.T. Zhu, F. Zhou, E.J. Lavernia, H.F. Xu, *Appl. Phys. Lett.* 84 (2004) 3564.